GeoStorage

Vol. 2, No. 1, p. 14-26, 2026

Research article

Analytical Assessment for Effective Activation Microcracks in Hydraulic Fracturing Influenced by Injection Rate of Compressive Brittle Rocks

Xiaozhao Li*, Haifeng Li, Zhuoxiang Zhang, Kairui Li, Chengzhi Qi

School of Civil and Transportation Engineering, Beijing University of Civil Engineering and Architecture, Beijing 100044, China

Keywords:
Brittle rock
hydraulic fracturing
hydraulic microcrack permeability
external injection flow rate
micro-macro fracture

Cited as:
Li XZ, Li HF, Zhang ZX, et al. 2026. Analytical Assessment for Effective Activation Microcracks in Hydraulic Fracturing Influenced by Injection Rate of Compressive Brittle Rocks. *GeoStorage*, 2(1), 14-26.
https://doi.org/10.46690/gs.2026.01.02

Abstract:
The injection rate in hydraulic fracturing exerts a profound influence on both fracturing efficiency and rock mechanical properties. However, existing research remains deficient in elucidating the mechanisms underlying the interplay between injection rate and microcrack-induced hydraulic fracturing in brittle rocks under triaxial compression. This study introduces a micro-macro fracture model to predict the effects of injection rate on hydraulic fracturing processes under such stress conditions. The model integrates the microcrack stress intensity factor (K_I), which is sensitive to the compressive stress state (σ_1, σ_3) and hydraulic pressure (P), with a fracture toughness (K_{IC}) function of single-crack injection rate (q) and pressure. A novel parameter, hydraulic microcrack permeability (k_q) representing the effective activation ratio of the initial microcracks, is proposed to correlate external injection rate (Q) with individual crack flow rate during hydraulic fracturing in brittle rocks. The model determines the evolution of hydraulic fracturing pressure with wing crack length induced by varying injection rates. Empirical validation confirms the robustness of the macro-fracture mechanics framework under diverse injection rates. Key findings indicate that increasing external injection rate inhibits the number of hydraulically activated initial microcracks and enhances the hydraulic peak pressure. The hydraulic initiation and peak pressures decrease with increasing axial load, stress differential, initial crack length, and density. Conversely, higher injection rates, confinement pressures, and initial crack angles result in elevated hydraulic peak pressure.

1 Introduction

Hydraulic fracturing, a pivotal reservoir stimulation technology, has been commercially implemented with proven efficacy in hydrocarbon recovery (Damjanac & Cundall, 2016; Chen et al., 2022a). This technology has found extensive applications across multiple engineering domains, including enhanced oil recovery, in-situ stress characterization, mine-induced structural response analysis, environmental remediation, and engineered geothermal systems (Davarpanah et al., 2019; Wan et al., 2019; Zhou et al., 2019; Yan et al., 2022; Meng & He, 2020; Kang et al., 2023; Xue et al., 2023; Yu et al., 2024). Particularly in shale gas extraction, hydraulic fracturing serves as the primary production enhancement method due to its cost-effectiveness, operational feasibility, and exceptional capability to expand fracture networks while improving formation permeability (Gomaa et al., 2014; Vengosh et al., 2014; Zhang et al., 2023).

The operational process of hydraulic fracturing uses surface-mounted high-pressure pumps to inject pressurized fluids through wellbores. When induced pressure exceeds the formation's fracture initiation threshold, rock failure generates conductive fractures (Ma et al., 2016). Effective implementation requires optimizing three key parameters: minimizing rock breakdown pressure, maximizing fracture network complexity, and controlling hydrocarbon extraction patterns to boost shale gas recovery (Gregory et al., 2011; Tang et al., 2018). However, shale gas extraction faces unique challenges due to

Yandy Scientific Press

* Corresponding author.
E-mail address: lixiaozhao@bucea.edu.cn (Li XZ); lihaifeng0095@126.com (Li HF); 2338016772@qq.com (Zhang ZX); likairui@bucea.edu.cn (Li KR); qichengzhi@bucea.edu.cn (Qi CZ)

Received Dec. 8, 2025; revised Dec. 28, 2025; accepted Jan. 2, 2026; available online Jan. 6, 2026.

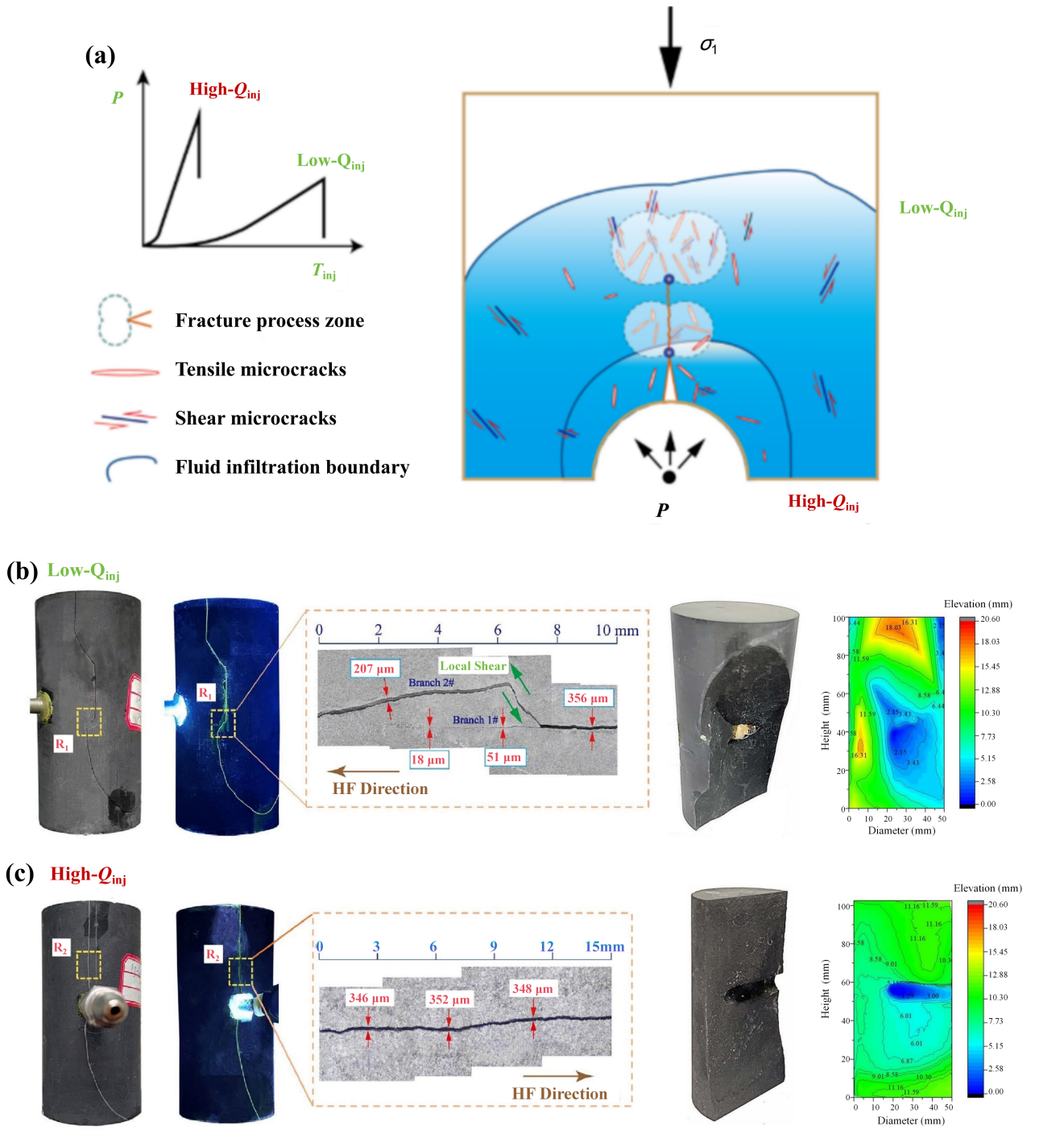

Fig. 1 (a) Schematic diagram and (b, c) experimental data of the hydraulic fracturing process zone formation with microcracks at low and high injection rates (Zhang et al., 2024)

ultra-low porosity-permeability and complex gas storage states. Key parameters influencing efficiency include horizontal stress differentials, rock brittleness indices, fracturing fluid rheology, and injection rate dynamics (Liu, 2005; Guo et al., 2014; Fan & Zhang, 2014; Bennour et al., 2015; Chen et al., 2015; Singh & Javadpour, 2016; Lin et al., 2017; Ranjith et al., 2018; Li & Einstein, 2019; Liu et al., 2020).

The external injection rate is closely linked to rock fracture pressure, though trends vary. Generally, lower fluid viscosity and injection rates reduce fracture pressure (Jia et al., 2021a,b; Morgan et al., 2017), but exceptions exist: experiments on tight gas-bearing sandstones and fulminate shales show higher rates can decrease fracture pressure (Zeng & Roegiers, 2002; Zhao et al., 2022a). For low-permeability rocks, tensile fracture and damage onset pressures are independent of pressurization rate, whereas higher-permeability rocks exhibit increased fracture pressure with faster injection, and the permeability itself cor-

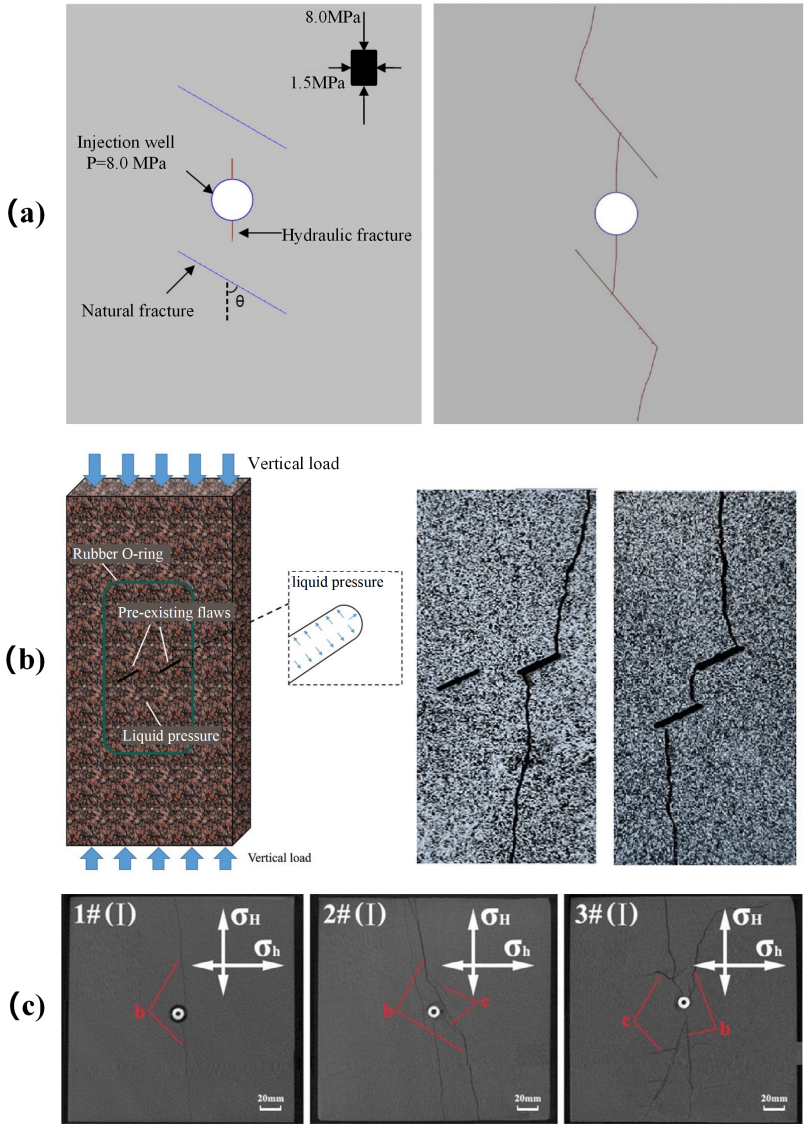

Fig. 2 The experiment basis for the new activated crack growing towards the direction of maximum principal compressive stress during hydraulic fracturing. a: Hydraulic-activated natural crack extension (Janiszewski et al., 2019), b: Hydraulic-activated pre-existing minor crack extension (Zhao et al., 2020), c: CT scanning plane of hydraulic-activated crack extension in rocks (Zhang et al., 2017)

relates with injection rate (Zoback et al., 1977; Solberg et al., 1980; Zhuang & Kim et al., 2019; Chen et al., 2022b). Injection rate also shapes fracture networks: lower rates form more complex microfractures, while higher rates reduce curvature and surface roughness (Fig. 1), critically influencing final morphology.

Different rock bodies exhibit distinct hydraulic fracturing behaviors even at identical external injection rates (Li & Einstein, 2019; Zhang et al., 2024). To mitigate leakage and boost production, increasing fluid friction, via higher injection rates or fracturing fluid viscosity, enhances pressurization (Beugelsdijk et al., 2000). In sandstone and coal seams, shot hole injection proves effective. It reduces near-wellbore fracture deformation, while horizontal fluid flow connects natural fractures to form networks, further improving production (Wang et al., 2019). Fallahzadeh et al. (Fallahzadeh et al., 2017) tested cubic samples under realistic far-field stress, finding that higher fluid viscosity and flow rate increase fracture initiation angles and drive more zigzag propagation. Guo et al. (Guo et al., 2014) simulated shale fracturing and showed that greater stress differences cause hydraulic fractures to intersect, creating complex systems. Under uniaxial stress, Zhao et al. (Zhao et al., 2022a) noted fracture pressure behaves differently than under conventional confining pressure, with anisotropy angle and flow rate also influencing it. Despite extensive study on how flow rate affects fracture morphology, the detailed mechanisms, including how varying rates shape fractures, remain underexplored.

In general, the mechanism of the external injection rate effect on the hydraulic fracturing triggered by the activated microcrack extension in brittle rocks is still unclear. In this paper,

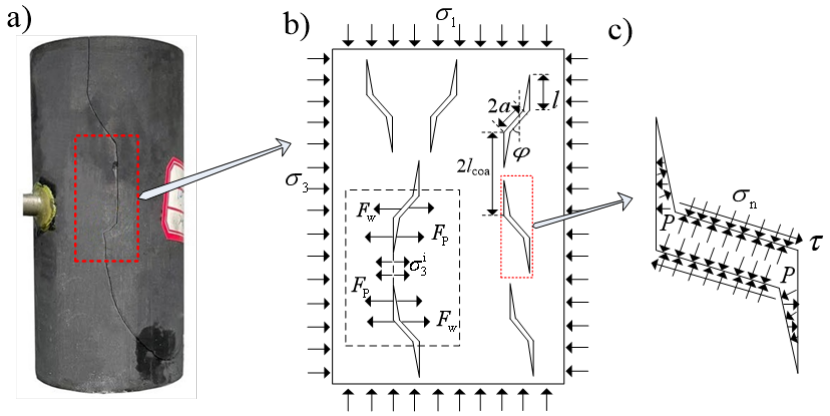

Fig. 3 a: Experimental plot of hydraulic fracturing in rock sample of Fig.1, b: equivalent model of the macroscopic hydraulic fracturing induced by internal activated microcrack expansions, and c: schematic of hydraulic pressure on individual crack in compressed brittle rock

the micro-macro fracture mechanics law of hydraulic fracturing in brittle rock will be investigated by combining the effects of external stress difference and external injection rate of fracturing fluid. The influence of the external injection rate on the hydraulic fracturing process will be explored by distributing the external injection rate equally into the permeable microcracks through the homogenization method in brittle rock. By analyzing and processing the experimental data, the correlation of the external injection rate, the hydraulic microcrack permeability, and the single microcrack injection rate will be obtained.

2 Analytical method formulation

2.1 Microcrack stress intensity factor coupling with hydraulic pressure in rocks

In this study, based on the fracture model triggered by numerous wing microcracks growth subjected to the compressive loadings (Ashby & Sammis, 1990; Li et al., 2018, 2024) and the experimental phenomena of hydraulic crack growing towards the maximum principal compression stress in Fig.2 (Janiszewski et al., 2019; Zhao et al., 2020), a model predicting the effect of injection flow rate on the hydraulic microcrack growth-derived brittle rock fracture under triaxial compression is constructed in Fig.3.

Fig.3a illustrates the multiple microcrack extension model containing the equalization assumptions of the microcrack geometry characteristics and the interaction of adjoining microcracks in brittle rock during hydraulic fracturing. It is unable to analyze the heterogeneity caused by the random distribution of microcracks within the rock. In this model, the average radius of each initial microcrack is defined as "a" and an average wing microcrack of length "l" extends from the end of each initial crack. The average angle between the initial microcrack and the direction of the maximum principal compressive stress σ_1 is set to φ, where α is equal to the cosine of φ. These specific average microcrack features of the rocks can define different types of brittle rocks (granite, marble, shale, etc.) that follow wing-shaped crack propagation characteristics. Under the pore water pressure, the force of individual cracks is shown in Fig. 3b. The lateral pressure σ_2 is equal to σ_3. For the analysis of the theoretical model, the compressive stresses (including the external compressive stress and the hydraulic pressure) are regarded as negative values, but for the convenience of observation, the pressures are expressed as positive values in the diagrams.

A mode-I stress intensity factor K_I for the tip of the internal wing crack in brittle rocks under hydraulic fracturing is proposed as (Li et al., 2024):

$$K_I = \frac{F_w}{[(\beta a + l)\pi]^{3/2}} + \frac{2(\sigma_3 + \sigma_3^i)\sqrt{\pi l}}{\pi} \tag{1}$$

Where

$$\sigma_3^i = \frac{F_w + F_p}{S - \pi(l + \alpha a)^2} \tag{2}$$

$$S = \pi^{1/3}\,[3/(4N_V)]^{2/3} \tag{3}$$

$$F_w = a^2\pi\tau\sin(\varphi) - ka^2\pi\sigma_n'\cos(\varphi) \tag{4}$$

$$F_p = -P\left[\pi(l + \alpha a)^2 - \pi(\alpha a)^2\right] \tag{5}$$

$$\tau = \frac{\sigma_3 - \sigma_1}{2}\sin(2\varphi) \tag{6}$$

$$\sigma_n' = \sigma_n - P = \frac{\sigma_1 + \sigma_3}{2} + \frac{\sigma_3 - \sigma_1}{2}\cos(2\varphi) - P \tag{7}$$

where β is the calibration factor, P is the hydraulic fracturing pressure or pore pressure, σ_n is the normal stress, σ_n' is the effective normal stress on the pre-crack plane, τ is the shear stress on the pre-crack plane, F_p is the tension on the wing crack surface due to the pore pressure, F_w is the wedge force at the prefabricated crack due to the external load, k is the folding factor of the stress at the crack tip during the cracking

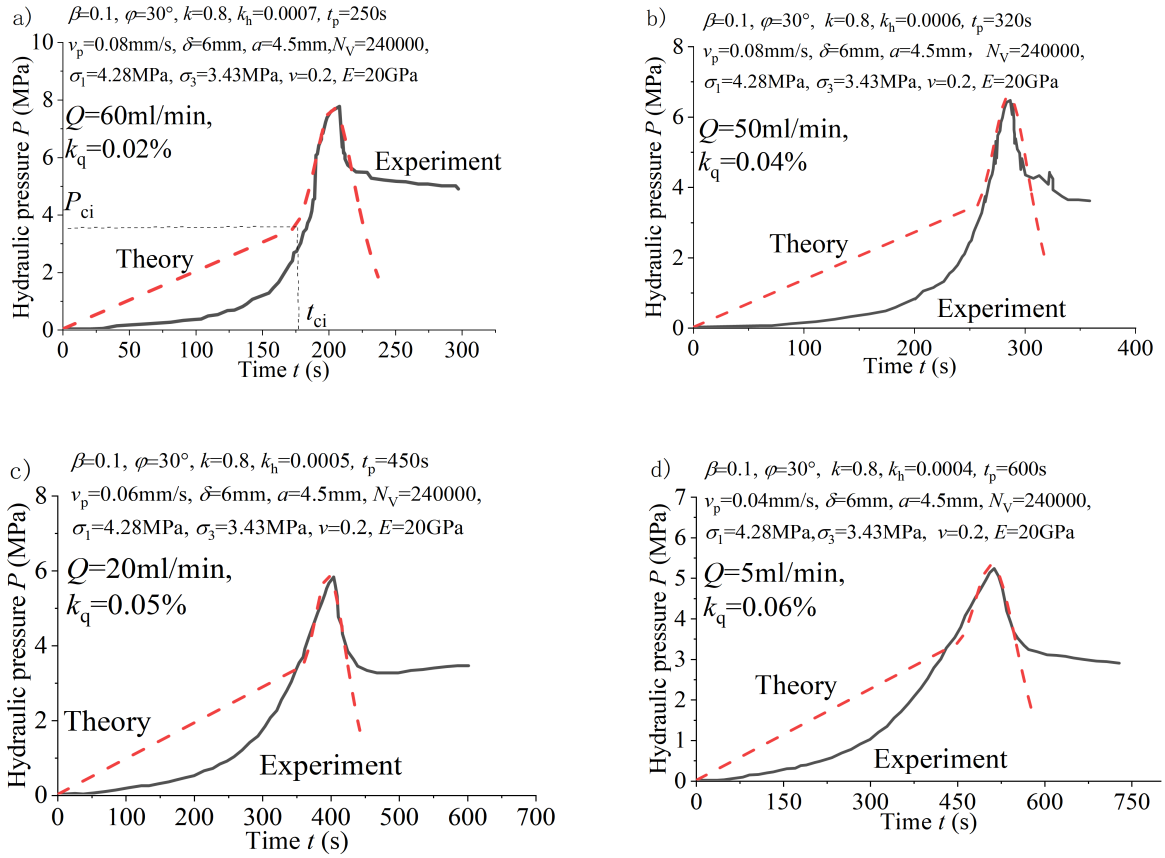

Fig. 4 Comparison of the proposed theoretical and the published experimental (Wang et al., 2019) at different injection flow rates a: Q=60ml/min, b: Q=50ml/min, c: Q=20ml/min, d: Q=5ml/min

surface opening (Li et al., 2024), σ_3^i is the internal stress acting at the crack tip, S is the occupied average area of individual microcrack surface. N_V is the number of initial cracks per unit volume of rock (i.e., initial crack density), the initial damage of rock is $D_0 = N_V a^3$, and the penetration length of winged cracks is $l_{coa} = (3/(4\pi N_V))^{1/3} - \alpha a$, which is auxiliary for evaluating the failure of rock. However, how the injection flow rate affects hydraulic fracturing is still unexplained by the above theoretical model, which will be discussed in the following.

2.2 Correlation of injection flow rate and hydraulic pressure in single cracking

Assuming that a hydraulically fractured crack obeys Griffith's law of energy balance at the moment of rupture, the correlation of the hydraulic fracturing pressure P of a single crack and the injection flow rate is shown in the following equation (Zeng & Roegiers, 2002):

$$P = \sqrt[3]{\frac{\pi\delta K_{IC}^4}{q t_p E'}} \tag{8}$$

where the plane strain modulus $E' = E/(1-\nu^2)$, δ is the fracture height in the borehole (i.e., the longitudinal fracture height in the initial microcrack of this study), K_{IC} is the fracture toughness of type I fracture, t_p is the fracture breakage time, ν is the Poisson's ratio, E is the Young's modulus, and q is the injection flow rate within a single crack. In practice, the fracturing fluid can't enter all the cracks, and different external injection flow rates lead to different fracture process zones inside the rock with different degrees of activation of the initial microcracks during hydraulic fracturing in Fig. 1. So, a key parameter of hydraulic microcrack permeability k_q is introduced by use of the experimental phenomena (Zhang et al. 2024) of Fig.2, and the external injection flow rate Q and the single microcrack injection flow rate q of brittle rocks can be suggested as:

$$q = \frac{Q}{k_q \cdot N_V} \tag{9}$$

where Q is the external injection rate. Since the parameter of hydraulic microcrack permeability k_q represents the activation of microcracks within the rock, it is difficult to directly observe and determine through experiments. The hydraulic microcrack permeability k_q will be inversely proportional to the external injection rate, which agrees with the experimental phenomena of Fig. 1. The specific value can be determined by fitting the theoretical and experimental curve in the hydraulic fracturing pressure of Figs. 4 and 5 below.

Eq. (8) is processed to inverse solve for fracture toughness

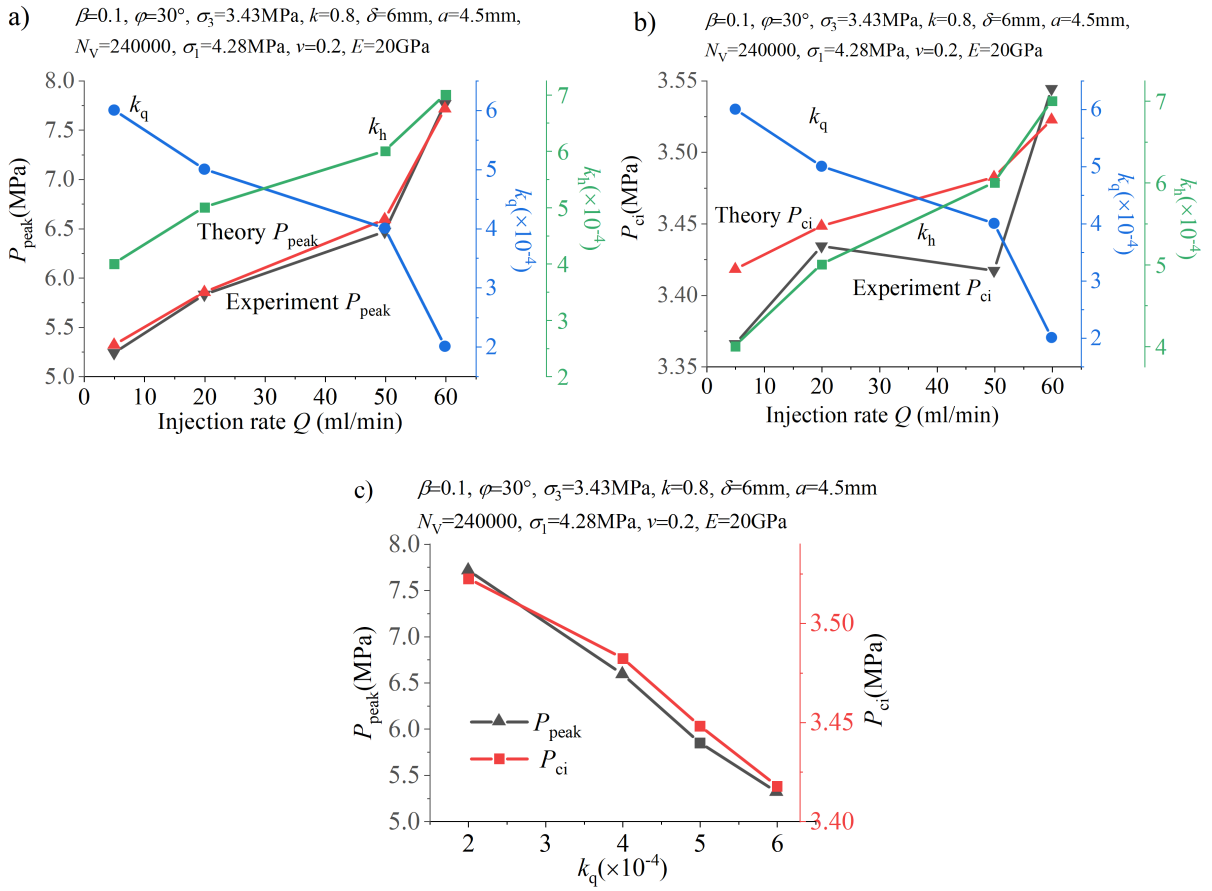

Fig. 5 The comparison of theoretical and experimental (Wang et al., 2019) results of the hydraulic. a: peak Ppeak, b: initial Pci stress, c: the variations of hydraulic peak and initial stress with the hydraulic microcrack permeability kq under different injection flow rates Q

K_{IC}:

$$K_{IC} = \sqrt[4]{\frac{P^3 q t_p E'}{\pi\delta}} = -k_h P \sqrt[4]{\frac{q t_p E'}{\pi\delta}} \tag{10}$$

where k_h is the weakening coefficient, with a value range of $0 < k_h < 0.2$. A simplification $k_h P = P^{3/4}$ is used to complete the derivation and calculation of the subsequent model and the specific value k_h will satisfy strictly the mathematical rule, which will also be further illustrated in the results of Fig.6 below.

2.3 Injection flow rate effect on hydraulic fracturing triggered by multi-cracking

When stress intensity factor K_I reaches to fracture toughness K_{IC}, wing crack growth appears. Substituting Eq. (10) into Eq. (1) and inversely solving for hydraulic pressure P, the wing crack growth-dependent hydraulic pressure considering the external injection flow rate Q can be proposed as:

$$P(l,Q) = \frac{A_5\left(2\sqrt{\frac{l}{\pi}}A_3 + A_2\right)A_4 + 2A_2A_3\sqrt{\frac{l}{\pi}}\sigma_3}{-k_h\sqrt[4]{\frac{Qt_pE'}{k_qN_v\pi\delta}} + 2\sqrt{\frac{l}{\pi}}A_3(A_4k + A_1) + A_2A_4k} \tag{11}$$

Where

$$A_1 = \pi\left[(l+\alpha\alpha)^2 - (\alpha\alpha)^2\right] \tag{12}$$

$$A_2 = (l+\alpha\beta)^3 \tag{13}$$

$$A_3 = S - \pi(l+\alpha\alpha)^2 \tag{14}$$

$$A_4 = \alpha^2\pi\cos(\varphi) \tag{15}$$

$$A_5 = k\sigma_3 - (\sigma_3 - \sigma_1)(k-1)\sin(\varphi)^2 \tag{16}$$

Equation (11) describes that the hydraulic pressure exhibits strengthening and softening phases as the wing crack growth. The hydraulic peak pressure P_{peak} can be determined from Eq. (11). When the wing crack length l equals zero, the hydraulic initiation pressure P_{ci} considering the external injection flow rate Q is proposed by the following equation:

$$P_{ci}(l=0,Q) = \frac{A_5A_4A_3}{-k_h\sqrt[4]{\frac{Qt_pE'}{k_qN_v\pi\delta}} + A_2A_4k} \tag{17}$$

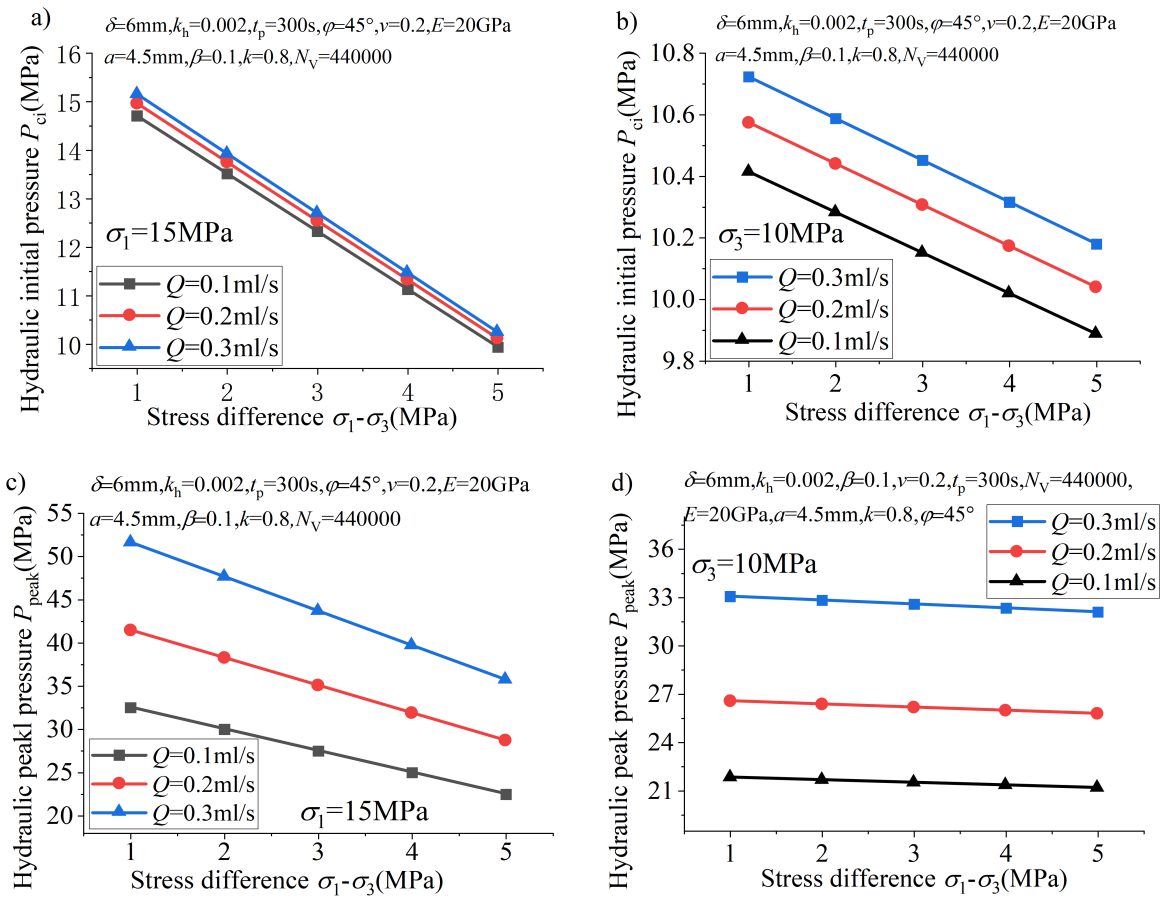

Fig. 6 Variations of hydraulic initiation P_{ci} and peak P_{peak} pressures for a) and c) the constant axial pressure σ_1, b) and d) the constant peripheral pressure σ_3 with stress differences under different external injection flow rates

The whole evolution process of hydraulic pressure during hydraulic fracturing can be comprehensively by combining the above Eqs. (11) and (17). Assuming an average crack growth rate of $v_p \approx l_{\text{coal}}/(t_p - t_{ci})$, the winged crack length is equal to the product of the time t and the average rate of crack growth, i.e., $l = v_p * t$. The parameter t_{ci} is the duration before hydraulic wing crack initiation, which can be determined approximately by the hydraulic fracturing test. The hydraulic pressure is assumed to linearly increase with time before wing crack initiation. The time before hydraulic wing crack initiation is included equivalently in the whole fracture breakage time t_p during hydraulic fracturing. The total time-dependent hydraulic pressure P with the effect of the external injection flow rate Q during hydraulic fracturing can be expressed as:

$$P(t,Q)=\begin{cases}\dfrac{P_{ci}}{t_{ci}}t=\dfrac{A_5A_4A_3t}{-k_h\sqrt[4]{\frac{Qt_pE'}{kq\nu_p\pi\delta}}+A_2A_4k}, & (0\le t\le t_{ci})\\ \dfrac{A_5\left(2\sqrt{\frac{v_pt}{\pi}}A_3+A_2\right)A_4+2A_2A_3\sqrt{\frac{v_pt}{\pi}}\sigma_3}{-k_h\sqrt[4]{\frac{Qt_pE'}{kq\nu_p\pi\delta}}+2\sqrt{\frac{v_pt}{\pi}}A_3(A_4k+A_1)+A_2A_4k}, & (t_{ci}<t\le t_p)\end{cases} \tag{18}$$

The model parameter values can be determined by fitting the theoretical and experimental curve of the time-dependent hydraulic pressure and referring to the values of the known styles of rocks (Ashby and Sammi,1990; Li et al. 2018, Li et al. 2024).

3 Model rationality verification

A comparison of the proposed theoretical predictions and the published experimental data (Wang et al., 2019) for the variation of hydraulic pressure with time is shown at different injection flow rates during hydraulic fracture in Fig.5. The model proposed in this study can elucidate the relationship between hydraulic pressure and microcrack extension under different flow rate conditions. As it is difficult to directly measure the specific length of microcracks inside the rock in the experiment, the experimental data mainly reflect the change of hydraulic pressure with time. To achieve a comparative analysis between theoretical and experimental data, an estimated average crack extension rate v_p is used in the theoretical model, which converts the length of crack extension into the time variable of crack opening. To make the theoretical predictions closer to the experimental results, different crack extension rates were chosen for the model under different external injection flow rate conditions.

In Fig. 4a, the external injection flow rate is Q = 60ml/min, the average crack extension rate is 0.08mm/s. After 175s of loading, the initial cracks reached the initiation state. In 175s

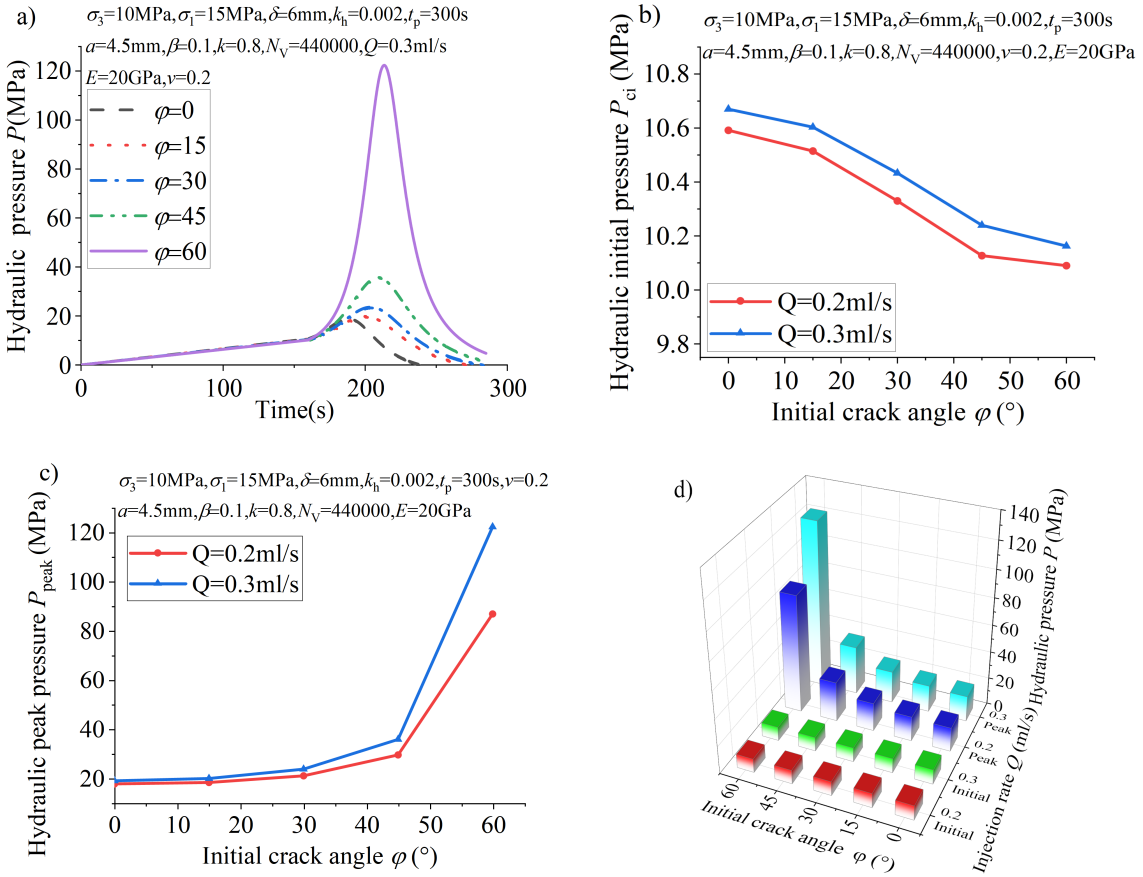

Fig. 7 Comparison of hydraulic fracturing under the effect of initial crack angle coupled with external injection flow rate for a) the whole process, b) the hydraulic initiation pressure P_{ci}, c) the hydraulic peak pressure P_{peak} and d) the three-dimensional trend

to 204s the rock went through the strengthening phase, reaching the stress peak condition. The water pressure rapidly decreased, the adjacent cracks gradually penetrated, and the rock failed after 204s of loading. In Fig. 4b, the external injection flow rate is Q = 50ml/min, the average crack rate is 0.08mm/s. After 258s of loading, the initial cracks reached the initiation state. In the process of loading 258s-286s, the rock undergoes the strengthening stage and reaches the stress maximum state, and after loading 286s, the hydraulic pressure decreases rapidly. In Fig. 4c, the external injection flow rate is Q = 20ml/min, the average cracking rate is 0.06mm/s. After 360s of loading, the initial cracks begin to crack. From 360 to 397 seconds, the rock enters a strengthening phase and reaches its peak pressure. After 397 seconds, the water pressure drops to zero. In Fig. 4d, the external injection flow rate is Q = 5ml/min, the average cracking rate is 0.04mm/s. After 455s of loading, the initial cracks begin to crack. From 455 to 510 seconds, the rock enters a strengthening phase and reaches its peak pressure. After 510 seconds, the water pressure drops to zero. The theoretical and experimental curves exhibit identical trends, demonstrating strong concordance about the hydraulic peak pressure.

Nonetheless, a notable discrepancy exists between the experimental and theoretical results in the change curve following the peak hydraulic pressure. In the theoretical model, the rock strength diminishes to 0 within a certain timeframe after the peak hydraulic pressure reaches the maximum penetration stress. Conversely, in the experimental observations, after attaining the peak penetration stress, the strength declines rapidly but ultimately retains a specific residual strength. This phenomenon may arise because the model presented in this paper fails to accurately replicate the stochastic distribution of the rock's cracking characteristics, relying solely on an averaging approach. Instead, it employs an averaging approach to analyze and simulate the hydraulic fracture process, assuming that all initial crack lengths and angles are average values. Furthermore, the model only accounts for the interaction between two adjacent wing cracks to represent the global failure characteristics of the rock, thereby neglecting the complex interactions of multiple cracks in anisotropic real rock conditions.

Fig. 5a, it can be found that hydraulic peak pressure increases with the increment of external injection flow rate. This agrees with the experiments conducted by scholars (Zoback et al., 1977; Wang et al., 2019; Zhuang & Kim et al., 2019; Cheng & Zhang, 2020; Zhang et al., 2023, 2024), where the fracturing fluid will be more prone to osmosis at lower external injection flow rates, leading to a softening effect on the rock, which reduces the rock strength, resulting in lower effective stresses. At low external injection flow rates, the increased fluid infil-

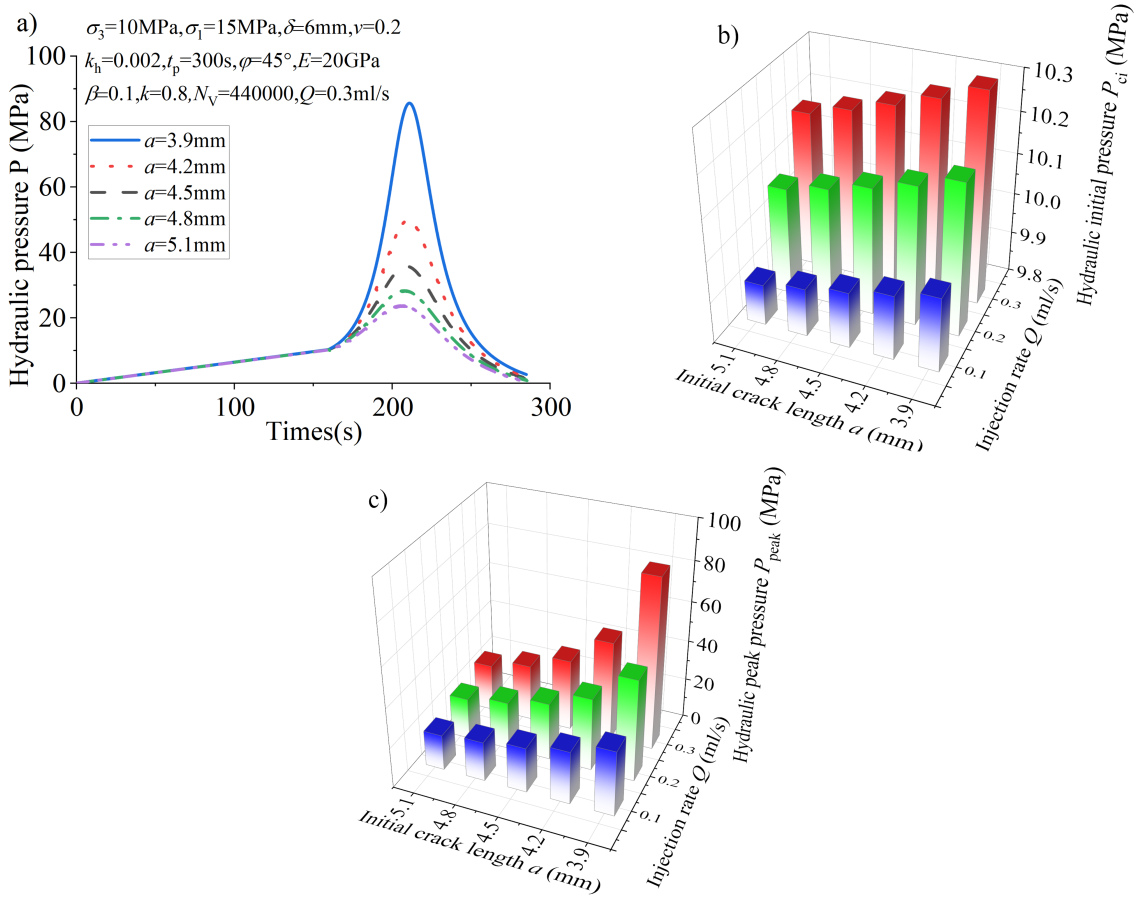

Fig. 8 Trends of hydraulic fracturing under the coupling effect of initial crack size and external injection flow rate for a) the whole process, b) the hydraulic initiation pressure P_{ci} and c) the hydraulic peak pressure P_{peak}

tration (i.e. the higher hydraulic microcrack permeability k_h) will increase pore fracturing, resulting in lower hydraulic peak pressure. At higher external injection flow rates, the elevated external injection flow rates will result in higher loading rates and reduced permeation of the fracturing fluid (i.e. the lower hydraulic microcrack permeability k_h), which will increase the hydraulic peak pressure. It can be concluded that the competitive effect between fluid permeation and loading rate controls the peak hydraulic pressure. At low external injection flow rates, the hydraulic peak pressure is mainly controlled by fluid permeation. In contrast, at high external injection flow rates, the hydraulic peak pressure is mainly controlled by the loading rate. In Fig. 5b, the hydraulic initial pressure increases with the increment of the external injection flow rate. However, the variation of hydraulic initial pressure with injection flow rate is smaller than that of hydraulic peak pressure. The experimental and theoretical curves are in better agreement on the overall trend. The hydraulic initial and peak pressures are shown in Figs.5 a and b are derived from the overall hydraulic fracturing process curves in Fig. 4. Furthermore, the weakening coefficient k_h increases with the increment of the external injection flow rate, which obeys calculated results from the basic mathematical simplification of Eq. (10).

From Figs. 5a and 5b, it can be observed that k_h shows a significant negative correlation with the external injection rate. This phenomenon indicates that when the external injection rate is high, the number of fractures that the fracturing fluid can enter is relatively small, which means that the number of softened fractures is correspondingly reduced. Higher external injection rates may lead to a non-uniform distribution of the fracturing fluid in the material, allowing only some cracks to be effectively softened, while others remain high. As fewer cracks are softened, the material requires greater penetrating water pressure to initiate crack expansion and cracking. As a result, at higher external injection rates, the material needs to be subjected to greater stresses as it reaches cracking conditions, leading to an increase in peak stress. Fig. 5c also shows a direct variation of the hydraulic peak and initial stress with the hydraulic microcrack permeability under different external injection flow rates.

This finding has important implications for understanding the mechanism of crack extension during fracturing and provides a theoretical basis for optimizing the parameters of the fracturing process, which is particularly valuable for practical applications in controlling the injection rate to regulate crack extension behavior. Furthermore, it is noted that this suggested key parameter of hydraulic microcrack permeability k_h is not measured directly by the experiment and is determined indirectly by fitting the proposed and experimental hydraulic pressure in Figs. 4 and 5.

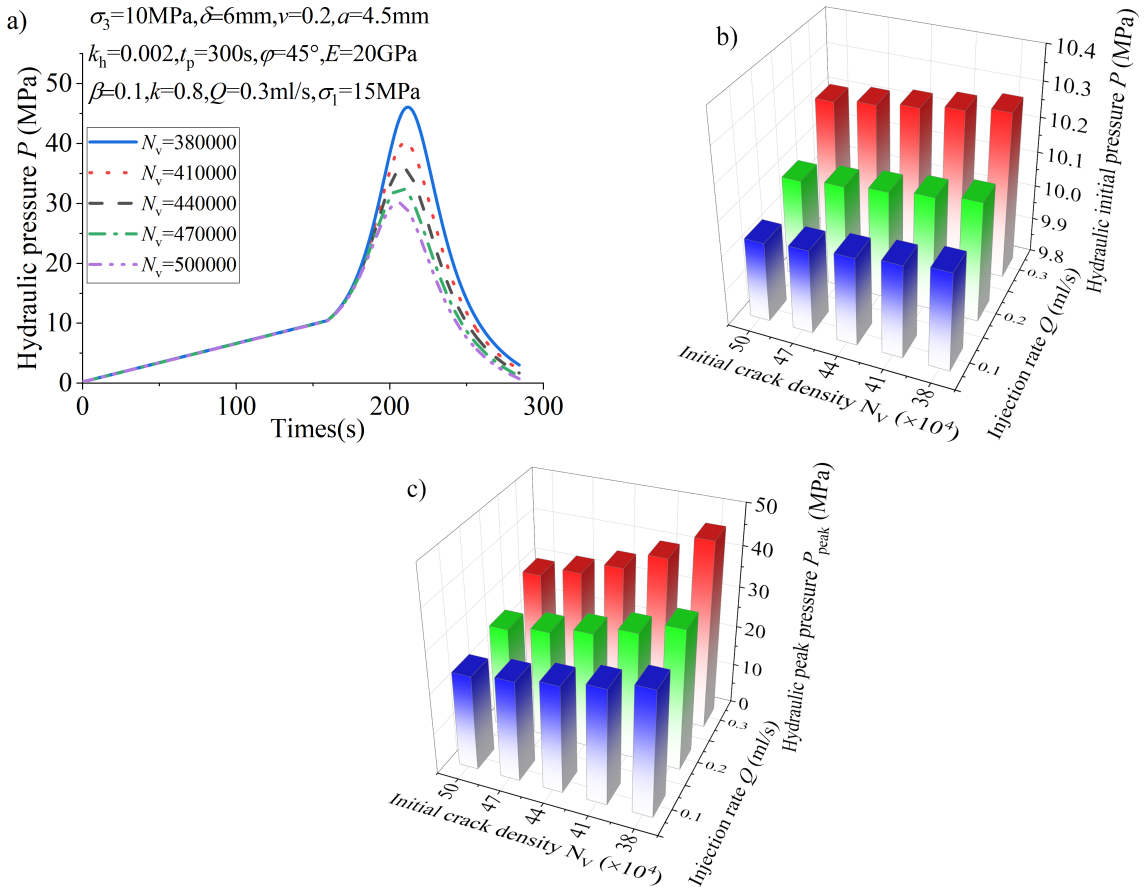

Fig. 9 Trends of hydraulic fracturing under the effect of density of initial crack coupled with external injection flow rate for a) the whole process, b) the hydraulic initiation pressure P_{ci} and c) the hydraulic peak pressure P_{peak}

While the study elucidates the mechanistic link between external injection rate and hydraulic fracturing behavior, where higher flow rates reduce fracturing fluid penetration range (limiting fracture morphology impact despite increased pore pressure gradients and peak pressure requirements) and lower flow rates expand penetration, reduce effective stress, activate more microcracks, and promote complex fracture networks via shear damage (Zhang et al., 2024), the connection to real-world engineering applications could be strengthened. Theoretically, the model introduces hydraulic microcrack permeability (k_q) to quantify how reduced flow rates enhance microcrack activation (Patel et al., 2017; Zhuang & Zang, 2021; Zhang et al., 2020a; Xie et al., 2020; Zhang et al., 2020b; Wang et al., 2021; Zhao et al., 2022b), altering macroscopic fracture paths, which can provide a demonstration of the model's practical utility in optimizing injection protocols through typical engineering scenarios. For instance, integrating field data from a shale gas well fracturing operation, such as comparing high/low flow rate protocols, microseismic monitoring of fracture complexity, or post-fracturing production data, would directly illustrate how the model guides parameter design to enhance reservoir stimulation efficiency. By briefly showcasing its application in such a scenario, the study could bridge theory and practice, highlighting how k_q-based insights might optimize injection strategies (e.g., staged flow rate adjustments) to balance fracture complexity and operational costs in real wells.

4 Discussions

The external initial stress state and microcrack characterization parameters of the rock significantly impact hydraulic fracturing. However, how the above mechanical properties are affected when considering the external injection flow rate needs further in-depth exploration. The hydraulic microcrack permeability $k_q = 5.622 \times 10^{-4}$ for $Q = 0.1$ml/s, $k_q = 4.082 \times 10^{-4}$ for $Q = 0.2$ml/s, $k_q = 3.384 \times 10^{-4}$ for $Q = 0.3$ml/s will be used in the discussions at these three external injection flow rates below.

4.1 Effect of stress difference coupled with external injection flow rate

When the axial pressure remains constant, with the decrease of the peripheral pressure, the hydraulic initiation and peak pressures both descend (as in Fig. 6a, c). When the peripheral pressure is certain, with the increase of the axial pressure, the hydraulic initiation and peak pressures both decrease (as in Fig. 6b, d). Fig.6 shows that as the stress difference gradually increases, the initial and peak hydraulic pressures of the rock show a decreasing trend. The axial pressure becomes the main

influencing factor and reduces the hydraulic fracturing capacity of the rock. The hydraulic initial and peak pressures rose as the external injection flow rate increased when the stress difference was kept constant.

4.2 Influence of initial crack angle coupled with external injection flow rate

As shown in Fig. 7a, the peak of the curve at 60° initial crack angle is much higher than the other curves, i.e. the increase of the initial crack angle causes the increment of hydraulic peak pressure (Fig.7c). As the angle of initial crack increases from 0° to 60°, the hydraulic initial pressure decreases gradually, which is due to the stress difference $\sigma_1 - \sigma_3$ of 5 MPa at this time (Fig.7b). Then, as the angle of initial crack increases from 0° to 90°, it increases when the initial stress difference is less than 3 MPa. The hydraulic initial pressure at the same angle increases as the external injection flow rate increases. The difference in peak pressure at different external injection flow rates increases as the angle of the initial crack increases (Fig.7c). The magnitude of the variation in the initial and peak hydraulic pressures as the initial crack angle increases at different external injection flow rates can be more visually observed in Fig.7d.

4.3 Effect of initial damage coupled to external injection flow rate

Initial crack length a and number N_V are the two central factors determining the degree of initial damage to the rock (i.e., $D_0 = N_V a^3$), and they have a great effect on the strength of the rock during the hydraulic fracturing process (Budiansky and O'Connel. , 1976). Suppose the hydraulic fracturing strength of a rock is evaluated only in terms of overall initial damage. In that case, the effect of microscopic crack characteristics on the results may not be adequately captured. Therefore, the specific effects of the length of initial crack and the number of initial cracks on the hydraulic fracturing strength of rocks must be examined separately to more accurately understand how these factors play a role in hydraulic fracturing effectiveness.

The hydraulic fracturing curves for different initial crack lengths at the same external injection flow rate are shown in Fig. 8a, where the hydraulic initial and peak pressure increase with the decreasing size of initial crack. When the external injection flow rate increases gradually, the hydraulic initial and peak pressure at the same initial crack length also increase with the increase of the external injection flow rate (Fig. 8b-c). The increase of hydraulic peak pressure becomes more obvious with the increase of external injection flow rate. It indicates that at lower external injection flow rates, the internal cracks in the rock are invaded by the fracturing fluid, which leads to the weakening of the rock itself, resulting in a lower hydraulic peak pressure.

The density and length of the initial cracks have different effects on the hydraulic fracturing strength of the rock. The hydraulic fracturing curves at five different initial crack densities are illustrated in Fig. 9a. Both the hydraulic peak and initial pressures increase as the initial crack density decreases, which is in contrast to Li et al. who suggested that the hydraulic initial pressure is not influenced by the density of initial crack (Li et al., 2024). This is because, in this paper, we consider that the microcrack permeability of the rock under the influence of the external injection rate is closely related to the parameters of the initial crack density of the rock. When the initial crack density is changed, the microcracks permeability is changed, which influences the hydraulic initial pressure of the rock to a certain extent. So, the peak hydraulic initial pressure increases with the decrease in initial crack density.

As shown in Fig. 9b-c, the hydraulic initial pressure and hydraulic peak pressure under the same initial crack density increase with the increase of the external injection flow rate when the rock parameters and external load are kept constant, and the changes of the hydraulic initial pressure and hydraulic peak pressure when the external injection flow rate increases from 0.1 ml/s to 0.2 ml/s are smaller than the changes of the external injection flow rate from 0.2 ml/s to 0.3 ml/s. This is because the penetration rate of the microscopic cracks decreases as the external injection flow rate increases isometrically, and the higher external injection flow rate increases the loading rate of hydraulic fracturing, increasing the hydraulic peak pressure.

5 Conclusions

This study establishes a micro-macro mechanical model for evaluating the external injection flow rate effect on the hydraulic fracturing of brittle rock. A crucial parameter of hydraulic microcrack permeability k_q linking the external injection flow rate Q with the single crack injection flow rate q is proposed. The main conclusions are as follows:

- During hydraulic fracturing, the internal cracks expand along with the maximum principal compressive pressure in the rock under external compression, and the hydraulic pressure ascends and then descends with crack expansion. The hydraulic initial and peak pressure ascend with the increase of the external injection flow rate Q.
- Hydraulic microcrack permeability k_q decreases with the increasing external injection flow rate. It means that the increment of external injection flow rate inhibits the number of activated microcracks triggering the hydraulic fracturing of rock.
- The hydraulic initial pressure shows a decreasing trend as the angle of initial crack increases, while the peak pressure increases. In addition, the higher the initial crack length and density, the lower the hydraulic initial and peak pressures. As the stress difference between the axial and confining stresses increases, the initial and peak hydraulic pressures of the rock decrease accordingly.

Acknowledgements

This work was supported by the National Natural Science Foundation of China (Grant Nos. 52438007, 51708016 and 12172036), the R&D program of Beijing Municipal Education Commission (Grant No.KM202110016014), and the Cultivation project Funds for Beijing University of Civil Engineering and Architecture (X24029).

Conflict of interest

The authors declare no competing interest.

References

Ashby MF, Sammis CG. 1990. The damage mechanics of brittle solids in compression. *Pure and Applied Geophysics*, **133**(3):489–521. doi:10.1007/BF00878002.

Bennour Z, Ishida T, Nagaya Y, Chen Y, Nara Y, Chen Q, Sekine K, Nagano Y. 2015. Crack extension in hydraulic fracturing of shale cores using viscous oil, water, and liquid carbon dioxide. *Rock Mechanics and Rock Engineering*, **48**(4):1463–1473. doi:10.1007/s00603-015-0774-2.

Beugelsdijk LJL, De Pater CJ, Sato K. 2000. Experimental hydraulic fracture propagation in a multi-fractured medium. In: *Proceedings of the SPE Asia Pacific Conference on Integrated Modelling for Asset Management*. doi:10.2118/59419-MS.

Budiansky B, O'Connel RJ. 1976. Elastic moduli of a cracked solid. International Journal of Solids and Structures. *International Journal of Solids and Structures*, **48**(12):81–97. doi:10.1016/0020-7683(76)90044-5.

Chen B, Barboza BR, Sun Y, Bai J, Thomas HR, Dutko M, Cottrell M, Li CF. 2022a. A Review of Hydraulic Fracturing Simulation. *Archives of Computational Methods in Engineering*, **29**(4):1–58. doi:10.1007/s11831-021-09653-z.

Chen L, Kang Q, Dai Z, Viswanathan HS, Tao W. 2015. Permeability prediction of shale matrix reconstructed using the elementary building block model. *Fuel*, **160**:346–356. doi:10.1016/j.fuel.2015.07.070.

Chen R, Nie ZY, Peng Y, Xu Y, Yao W. 2022b. A dynamic hydraulic fracturing test technology based on split Hopkinson pressure bar system. *Experimental Mechanics*, **62**:813–822. doi:10.1007/s11340-022-00827-9.

Cheng Y, Zhang Y. 2020. Hydraulic fracturing experiment investigation for the application of geothermal energy extraction. *ACS Omega*, **5**(15):8667–8686. doi:10.1021/acsomega.0c00172.

Damjanac B, Cundall P. 2016. Application of distinct element methods to simulation of hydraulic fracturing in naturally fractured reservoirs. *Computers and Geotechnics*, **71**:283–294. doi:10.1016/j.compgeo.2015.06.007.

Davarpanah A, Shirmohammadi R, Mirshekari B, Aslani A. 2019. Analysis of hydraulic fracturing techniques: hybrid fuzzy approaches. *Arabian Journal of Geosciences*, **12**(13):402. doi:10.1007/s12517-019-4567-x.

Fallahzadeh SH, Hossain M, James Cornwell A, Rasouli V. 2017. Near wellbore hydraulic fracture propagation from perforations in tight rocks: the roles of fracturing fluid viscosity and injection rate. *Energies*, **10**:359. doi:10.3390/en10030359.

Fan TG, Zhang GQ. 2014. Laboratory investigation of hydraulic fracture networks in formations with continuous orthogonal fractures. *Energy*, **74**:164–173. doi:10.1016/j.energy.2014.05.037.

Gomaa AM, Qu Q, Maharidge R, Nelson S, Reed T. 2014. New insights into hydraulic fracturing of shale formations. In: *Society of Petroleum Engineers - International Petroleum Technology Conference 2014, IPTC 2014: Unlocking Energy Through Innovation, Technology and Capability*. doi:10.2523/iptc-17594-ms.

Gregory KB, Vidic RD, Dzombak DA. 2011. Water management challenges associated with the production of shale gas by hydraulic fracturing. *Elements*, **7**(3):181–186. doi:10.2113/gselements.7.3.181.

Guo T, Zhang S, Qu Z, Zhou T, Xiao Y, Gao J. 2014. Experimental study of hydraulic fracturing for shale by stimulated reservoir volume. *Fuel*, **128**:373–380. doi:10.1016/j.fuel.2014.03.029.

Janiszewski M, Shen B, Rinne M. 2019. Simulation of the interactions between hydraulic and natural fractures using a fracture mechanics approach. *Journal of Rock Mechanics and Geotechnical Engineering*, **11**(6):1138–1150. doi:10.1016/j.jrmge.2019.07.004.

Jia Y, Lu Z, Xiong Q, Hampton JC, Zhang Y, He P. 2021a. Laboratory characterization of cyclic hydraulic fracturing for deep shale application in Southwest China. *International Journal of Rock Mechanics and Mining Sciences*, **148**:104945. doi:10.1016/j.ijrmms.2021.104945.

Jia Y, Song C, Wang J, Gan Q. 2021b. The breakdown process of low-permeable shale and high-permeable sandstone rocks due to non-aqueous fracturing: the role of fluid infiltration. *Journal of Natural Gas Science and Engineering*, **89**:103873. doi:10.1016/j.jngse.2021.103873.

Kang H, Jiang P, Feng Y, Gao F, Zhang Z, Liu X. 2023. Application of Large-Scale Hydraulic Fracturing for Reducing Mining-Induced Stress and Microseismic Events: A Comprehensive Case Study. *Rock Mechanics and Rock Engineering*, **56**(2):1399–1413. doi:10.1007/s00603-022-03061-w.

Li BQ, Einstein HH. 2019. Direct and Microseismic observations of hydraulic fracturing in Barre granite and Opalinus clay shale. *Journal of Geophysical Research: Solid Earth*, **124**(11):11900–11916. doi:10.1029/2019JB018376.

Li XZ, Li HF, Qi CZ, Wu K. 2024. A micro-macro mechanism of hydraulic fracturing with initial stress state effect of brittle rock. *Geoenergy Science and Engineering*, **241**:213185. doi:10.1016/j.geoen.2024.213185

Li XZ, Qi CZ, Shao ZS. 2018. A microcrack growth-based constitutive model for evaluating transient shear properties during brittle creep of rocks. *Engineering Fracture Mechanics*, **194**:9–23. doi:10.1016/j.engfracmech.2018.02.034.

Lin C, He J, Li X, Wan X, Zheng B. 2017. An experimental investigation into the effects of the anisotropy of shale on hydraulic fracture propagation. *Rock Mechanics and Rock Engineering*, **50**:543–554. doi:10.1007/s00603-016-1136-4.

Liu E. 2005. Effects of fracture aperture and roughness on hydraulic and mechanical properties of rocks: implication of seismic characterization of fractured reservoirs. *Journal of Geophysics and Engineering*, **2**(1):38. doi:10.1088/1742-2132/2/1/006.

Liu J, Liang X, Xue Y, Fu Y, Yao K, Dou F. 2020. Investigation on crack initiation and propagation in hydraulic fracturing of bedded shale by hybrid phase-field modeling. *Theoretical and Applied Fracture Mechanics*, **108**:102651. doi:10.1016/j.tafmec.2020.102651.

Ma S, Guo J, Li L, Xia Y, Yang T. 2016. Experimental and numerical study on fracture propagation near open-hole horizontal well under hydraulic pressure. *European Journal of Environmental and Civil Engineering*, **20**(4):412–430. doi:10.1080/19648189.2015.1039661.

Meng W, He C. 2020. Back analysis of the initial geo-stress field of rock masses in high geo-temperature and high geo-stress. *Energies*, **13**(2):363. doi:10.3390/en13020363.

Morgan SP, Li BQ, Einstein HH. 2017. Effect of injection rate on hydraulic fracturing of Opalinus clay shale. In: *51st US Rock Mechanics / Geomechanics Symposium 2017*.

Patel SM, Sondergeld CH, Rai CS. 2017. Laboratory studies of hydraulic fracturing by cyclic injection. *International Journal of Rock Mechanics and Mining Sciences*, **95**:8–15.

doi:10.1016/j.ijrmms.2017.03.008.

Ranjith PG, Wanniarachchi WAM, Perera MSA, Rathnaweera TD. 2018. Investigation of the effect of foam flow rate on foam-based hydraulic fracturing of shale reservoir rocks with natural fractures: an experimental study. *Journal of Petroleum Science and Engineering*, **169**:518–531. doi:10.1016/j.petrol.2018.06.002.

Singh H, Javadpour F. 2016. Langmuir slip-Langmuir sorption permeability model of shale. *Fuel*, **164**:28–37. doi:10.1016/j.fuel.2015.09.073.

Solberg P, Lockner D, Byerlee JD. 1980. Hydraulic fracturing in granite under geothermal conditions. *International Journal of Rock Mechanics and Mining Sciences*, **17**:25–33. doi:10.1016/0148-9062(80)90003-0.

Tang H, Li S, Zhang D. 2018. The effect of heterogeneity on hydraulic fracturing in shale. *Journal of Petroleum Science and Engineering*, **162**:292–308. doi:10.1016/j.petrol.2017.12.020.

Vengosh A, Jackson RB, Warner N, Darrah TH, Kondash A. 2014. A critical review of the risks to water resources from unconventional shale gas development and hydraulic fracturing in the United States. *Environmental Science & Technology*, **48**(15):8334–8348. doi:10.1021/es405118y.

Wan L, Hou B, Tan P, Chang Z, Muhadasi Y. 2019. Observing the effects of transition zone properties on fracture vertical propagation behavior for coal measure strata. *Journal of Structural Geology*, **126**:69–82. doi:10.1016/j.jsg.2019.05.005.

Wang J, Xie H, Li C. 2021. Anisotropic failure behaviour and breakdown pressure interpretation of hydraulic fracturing experiments on shale. *International Journal of Rock Mechanics and Mining Sciences*, **142**:104748. doi:10.1016/j.ijrmms.2021.104748.

Wang Y, Zhang D, Hu YZ. 2019. Laboratory investigation of the effect of injection rate on hydraulic fracturing performance in artificial transversely laminated rock using 3D laser scanning. *Geotechnical and Geological Engineering*, **37**:2121–2133. doi:10.1007/s10706-018-0749-7.

Xie Q, Li S, Liu X, Gong F, Li X. 2020. Effect of loading rate on fracture behaviors of shale under mode I loading. *Journal of Central South University*, **27**:3118–3132. doi:10.1007/s11771-020-4533-5.

Xue Y, Liu S, Chai J, Liu J, Ranjith PG, Cai C, Gao F, Bai X. 2023. Effect of water-cooling shock on fracture initiation and morphology of high-temperature granite: Application of hydraulic fracturing to enhanced geothermal systems. *Applied Energy*, **337**:120858. doi:10.1016/j.apenergy.2023.120858.

Yan C, Chen Y, Chen T, Cheng Y, Yan X. 2022. Experimental Study of Hydraulic Fracturing for Unconsolidated Reservoirs. *Rock Mechanics and Rock Engineering*, **55**(6):3399–3424. doi:10.1007/s00603-022-02827-6.

Yu JJ, Li NY, Hui B, Zhao W, Li Y, Kang J, Hu P, Chen Y. 2024. Experimental simulation of fracture propagation and extension in hydraulic fracturing: A state-of-the-art review. *Fuel*, **363**:131021. doi:10.1016/j.fuel.2024.131021.

Zeng Z, Roegiers JC. 2002. Experimental observation of injection rate influence on the hydraulic fracturing behavior of a tight gas sandstone. In: *SPE/ISRM Rock Mechanics Conference*. SPE, SPE-78172-MS. doi:10.2118/78172-MS.

Zhang X, Lu Y, Tang J, Zhou Z, Liao Y. 2017. Experimental study on fracture initiation and propagation in shale using supercritical carbon dioxide fracturing. *Fuel*, **190**:370–378. doi:10.1016/j.fuel.2016.10.120.

Zhang Q, Fan X, Chen P, Ma T, Zeng F. 2020a. Geomechanical behaviors of shale after water absorption considering the combined effect of anisotropy and hydration. *Engineering Geology*, **269**:105547. doi:10.1016/j.enggeo.2020.105547.

Zhang Y, Zhao Y, Zang A, Long Anfa. 2024. Acoustic emission evolution and hydraulic fracture morphology of Changning shale stressed to failure at different injection rates in the laboratory. *Rock Mechanics and Rock Engineering*, **57**(2):1287–1308. doi:10.1007/s00603-023-03586-8.

Zhang Y, Long A, Zhao Y, Zang A, Wang C. 2023. Mutual impact of true triaxial stress, borehole orientation and bedding inclination on laboratory hydraulic fracturing of Lushan shale. *Journal of Rock Mechanics and Geotechnical Engineering*, **15**(12):3131–3147. doi:10.1016/j.jrmge.2023.02.015.

Zhang Y, Zhao Y, Yang H, Wang C. 2020b. A semianalytical solution for a Griffith crack nonuniformly pressurized by internal fluid. *Rock Mechanics and Rock Engineering*, **53**:2439–2460. doi:10.1007/s00603-020-02052-z.

Zhao C, Xing J, Zhou Y, Shi Z, Wang G. 2020. Experimental investigation on hydraulic fracturing of granite specimens with double flaws based on DIC. *Engineering Geology*, **267**:105510. doi:10.1016/j.enggeo.2020.105510.

Zhao Y, Zhang Y, Wang C, Liu Q. 2022a. Hydraulic fracturing characteristics and evaluation of fracturing effectiveness under different anisotropic angles and injection rates: an experimental investigation in absence of confining pressure. *Journal of Natural Gas Science and Engineering*, **97**:104343. doi:10.1016/j.jngse.2021.104343.

Zhao Y, Zhang YF, Tian GD, Wang CL, Bi J. 2022b. A new model for predicting hydraulic fracture penetration or termination at an orthogonal interface between dissimilar formations. *Petroleum Science*, **19**(6):2810–2829. doi:10.1016/j.petsci.2022.08.002.

Zhou L, Su X, Lu Y, Ge Z, Zhang Z, Shen Z. 2019. A new three-dimensional numerical model based on the equivalent continuum method to simulate hydraulic fracture propagation in an underground coal mine. *Rock Mechanics and Rock Engineering*, **52**(8):2871–2887. doi:10.1007/s00603-018-1684-x.

Zhuang L, Kim KY, Jung SG, Diaz M, Min KB. 2019. Effect of water infiltration, injection rate and anisotropy on hydraulic fracturing behavior of granite. *Rock Mechanics and Rock Engineering*, **52**:575–589. doi:10.1007/s00603-018-1431-3.

Zhuang L, Zang A. 2021. Laboratory hydraulic fracturing experiments on crystalline rock for geothermal purposes. *Earth-Science Reviews*, **216**:103580. doi:10.1016/j.earscirev.2021.103580.

Zoback MD, Rummel F, Jung R, Raleigh CB. 1977. Laboratory hydraulic fracturing experiments in intact and pre-fractured rock. *International Journal of Rock Mechanics and Mining Sciences*, **14**(2):49–58. doi:10.1016/0148-9062(77)90196-6.